

# First-principles Calculations of Raman and Infrared Spectroscopy For Phase Identification and Strain Calibration of Hafnia.

Aldo Raelarijaona<sup>a)</sup> and R. E. Cohen<sup>b)</sup>

*Extreme Materials Initiative, Earth and Planets Laboratory, Carnegie Institution for Science,  
5241 Broad Branch Road NW, Washington, DC 20015, USA*

(Dated: 13 June 2022)

Using density functional perturbation theory (DFPT) we computed the phonon frequencies, Raman and IR activities of hafnia polymorphs (P4<sub>2</sub>nmc, Pca2<sub>1</sub>, Pmn2<sub>1</sub>, Pbca OI, brookite, and baddeleyite) for phase identification. We investigated the evolution of Raman and IR activities with respect to epitaxial strain and provide plots of frequency differences as a function of strain for experimental calibration and identification of the strain state of the sample. We found Raman signatures of different hafnia polymorphs:  $\omega(A_{1g}) = 300 \text{ cm}^{-1}$  for P4<sub>2</sub>nmc,  $\omega(A_1) = 343 \text{ cm}^{-1}$  for Pca2<sub>1</sub>,  $\omega(B_2) = 693 \text{ cm}^{-1}$  for Pmn2<sub>1</sub>,  $\omega(A_g) = 513 \text{ cm}^{-1}$  for Pbca (OI),  $\omega(A_g) = 384 \text{ cm}^{-1}$  for brookite, and  $\omega(A_g) = 496 \text{ cm}^{-1}$  for baddeleyite. We also identified the Raman  $B_{1g}$  mode, an anti-phase vibration of dipole moments, ( $\omega(B_{1g}) = 758 \text{ cm}^{-1}$  for OI,  $\omega(B_{1g}) = 784 \text{ cm}^{-1}$  for brookite) as the Raman signature of antipolar Pbca structures. We calculated a large splitting between longitudinal optical (LO) and transverse optical (TO) modes ( $\Delta\omega_{\text{LO-TO}}(A_1^z) = 255 \text{ cm}^{-1}$  in Pca2<sub>1</sub>, and  $\Delta\omega_{\text{LO-TO}}(A_1) = 263 \text{ cm}^{-1}$  in Pmn2<sub>1</sub>) to the same order as those observed in perovskite ferroelectrics, and related them to the anomalously large Born effective charges of Hf atoms ( $Z^*(\text{Hf}) = 5.54$ ).

Hafnia is of great interest because of its compatibility with silicon and its robust ferroelectricity at the nanoscale. It has a high permittivity and has been proposed as a dielectric material for dynamic random access memories (DRAM) and logic devices<sup>1,2</sup>. At ambient pressure and temperature it stabilizes in the monoclinic crystal structure (P2<sub>1</sub>/c)<sup>3</sup>, but can also have different structures depending on temperature and pressure. At ambient pressure there are two high-temperature polymorphs: the tetragonal (P4<sub>2</sub>nmc), when  $1700^\circ\text{C} < T < 2600^\circ\text{C}$ , and the cubic ( $Fm\bar{3}m$ ) when  $T > 2600^\circ\text{C}$ <sup>4</sup>. Other phases have been stabilized under different pressure, such as Pbca, when  $5.9 \text{ GPa} < P < 15 \text{ GPa}$ , and Pnma when under  $P > 15 \text{ GPa}$ <sup>4,5</sup>, epitaxial strain<sup>6</sup>, or doping<sup>7,8</sup>.

Recent investigations have highlighted the possibility and importance of ferroelectricity in hafnia<sup>9-14</sup>, and studies of yttrium-doped hafnia revealed the Pca2<sub>1</sub> polymorph as the polar phase responsible for ferroelectricity<sup>15</sup>. Antiferroelectricity has also been observed in doped hafnia<sup>16</sup> and further theoretical studies have shown that the orthorhombic Pbca structure, which contains two Pca2<sub>1</sub> cells with opposite oxygen displacement relative to the hafnia atoms, as the antiferroelectric orthorhombic structure<sup>11</sup>. Hafnia is also of fundamental interest due to its fluorite-based structure, different from the wide class of well-studied perovskite ferroelectrics. One hindrance to the rapid development of hafnia ferroelectrics has been a lack of basic understanding of ferroelectricity.

Structural studies are usually based on X-ray diffraction (XRD) methods. Complementary to XRD, inelastic

light scattering such as Raman or IR spectroscopy is also a tool that can be used to determine the structure and structural response of different hafnia phases. The latter approach reveals information about interatomic interaction, hence atomic arrangements, through the vibrational spectra. Epitaxial strain is important in thin films and it can affect the Raman frequencies and intensities. One of the advantages of Raman spectroscopy is that it can provide information about the strain on the sample once calibrated. Only Raman shifts and peak intensities are accessible experimentally thus the need of first-principles studies of atomic vibrations for symmetry assignment of Raman peaks. Although Raman and IR data are available from previous calculations of hafnia polymorphs<sup>17-19</sup> they do not cover all the relevant phases, namely both polar orthorhombic phases or both antipolar orthorhombic phases. Furthermore, experimentally it is normal to observe mixture of different phases in hafnia such as baddeleyite and Pca2<sub>1</sub><sup>20</sup>, which makes the symmetry determination using Raman or IR spectroscopy crucial.

Our aim in this paper is to provide tools for experiments to identify the structure of hafnia and determine the epitaxial strain to which the sample is subject. Using DFPT we computed the phonon frequencies and their activities (Raman and IR) at different strain values ( $\eta = [-3.0\%, -1.5\%, 0.0\%, 1.5\%, 3.0\%]$ ) for different hafnia polymorphs, namely baddeleyite, P4<sub>2</sub>nmc, Pmn2<sub>1</sub>, Pca2<sub>1</sub>, Pbca (OI), and brookite. We tracked the evolution of phonon mode frequencies under strain, and provided means to identify the strain through identification of strain-induced frequency shifts of signature phonons.

We performed first-principles calculations using QUANTUM ESPRESSO<sup>21-23</sup>, with optimized norm-conserving Vanderbilt (ONCV) pseudopotentials<sup>24</sup>. The cell parameters and atomic positions were optimized using the local density approximation (LDA) with the Perdew-Zunger (PZ) exchange-correlation functional<sup>25</sup>,

<sup>a)</sup> Author to whom correspondence should be addressed: Aldo Raelarijaona, araeliarijaona@carnegiescience.edu

<sup>b)</sup> Electronic mail: rcohen@carnegiescience.edu

generated using the ONCVSP code<sup>24</sup>. The plane-wave expansion is truncated using a cutoff energy of  $E_{\text{cutoff}} = 1306.6$  eV, and the Brillouin zone was sampled using an  $8 \times 8 \times 8$  Monkhorst-Pack grid<sup>26</sup>. We calculated the Brillouin zone center phonon frequencies using density functional perturbation theory (DFPT)<sup>27</sup> implemented in the QE/PH package<sup>21–23</sup>. We considered the powder Raman spectra, with the Raman activity computed using Placzek approximation<sup>28–30</sup>. We plotted the spectra by convoluting with a Gaussian shape function whose width is  $5 \text{ cm}^{-1}$  estimated from experiments. Similar widths have been used in previous studies<sup>30</sup>.

We set a coordinate system similar to the ones defined in Ref.6. We consider the epitaxy of the tetragonal case with a square substrate such as Yttria-stabilized zirconia (YSZ), with  $\mathbf{z}$  normal to the epitaxial plane, and  $\mathbf{a}$  and  $\mathbf{b}$  in registry with the epitaxial surface. Strain  $\eta$  was applied by setting:

$$a_\eta = (1 + \eta)a_0, \quad (1)$$

where  $a_0$  is the strain-free ground state lattice constant of the tetragonal phase. The out-of-plane lattice constant ( $c$ ) and the atomic positions were relaxed at each strain.

To validate the accuracy of our DFPT calculations, we compare the calculated Raman spectra of the strain-free baddeleyite and brookite to the measured Raman spectra<sup>31</sup> (Fig.1). The Raman spectrum of brookite<sup>31</sup> was measured from a sample under hydrostatic pressure of  $P = 5.9$  GPa. So, for fair comparison, the cell parameters and the atomic positions for our calculations for brookite were relaxed under the same pressure. The calculated spectra of baddeleyite and brookite match the experimentally measured spectra well (Fig.1). For baddeleyite, the high intensity  $A_g$  peaks ( $\omega(A_g) = 495 \text{ cm}^{-1}$ ), the shoulder peak  $B_g$  ( $\omega(B_g) = 510 \text{ cm}^{-1}$ ), and the double peaks  $B_g$  ( $\omega(B_g) = 637 \text{ cm}^{-1}$ ) and  $A_g$  ( $\omega(A_g) = 670 \text{ cm}^{-1}$ ) all closely match with experimental peaks; for brookite we can point to the high intensity  $A_g$  peak ( $\omega(A_g) = 384 \text{ cm}^{-1}$ ), the  $B_{1g}$  peak ( $\omega(B_{1g}) = 513 \text{ cm}^{-1}$ ), the double peaks  $B_{3g}$  ( $\omega(B_{3g}) = 593 \text{ cm}^{-1}$ ) and  $B_{1g}$  ( $\omega(B_g) = 604 \text{ cm}^{-1}$ ). Our calculated spectra for baddeleyite, tetragonal and brookite also compare well with other calculations<sup>17,18</sup> (see Supplementary Material Fig.S1).

We plot the Raman spectra of the different strain-free hafnia polymorphs (Fig.1, Fig.2) to help with the identification of the crystal structures. The high intensity peaks of the Raman spectra can help in the identification of the structure symmetry. For example, the high intensity mode at  $\omega(A_g) = 496 \text{ cm}^{-1}$  is found only in baddeleyite. The  $\text{Pmn}2_1$  structure can be identified using the high frequency  $B_2$  ( $\omega(B_2) = 693 \text{ cm}^{-1}$ ) and  $A_1$  ( $\omega(A_1) = 722 \text{ cm}^{-1}$ ) peaks. The  $\text{Pca}2_1$  structure can be identified using the  $A_1$  peak ( $\omega = 340 \text{ cm}^{-1}$ ) and the strong  $A_1$  peak ( $\omega = 670 \text{ cm}^{-1}$ ). The presence of these peaks can be used to identify the  $\text{Pca}2_1$  structure. This is an advantage of the Raman (or IR) spectroscopy over the XRD given that phase identification using XRD

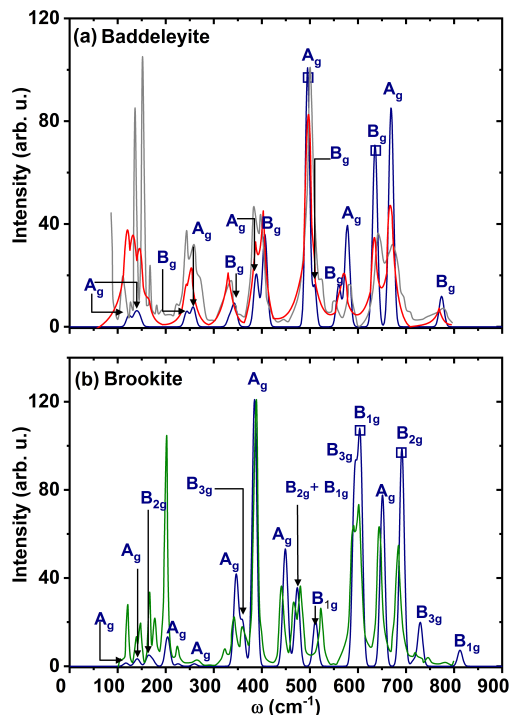


FIG. 1. Raman spectra of (a) baddeleyite, (b) brookite compared to experimental and theoretical Raman. Gray and green spectra are experimental data from Ref.31 and the red curve is a theoretical spectrum from Ref.17. We convoluted the spectra with a Gaussian shape function of width  $5 \text{ cm}^{-1}$  estimated from experiments. The squares indicate modes chosen to compute the frequency differences (Fig.4). For brookite Raman spectra (b), the blue and green curves were obtained under hydrostatic pressure ( $P = 5.9$  GPa).

can be harder due to the monoclinic and  $\text{Pca}2_1$  phase mixtures and the overlap of XRD peaks<sup>20</sup>, whereas with Raman spectroscopy the difference can be resolved easily. In  $\text{Pbca}$  (OI) the signature modes are the strong  $A_g$  peaks at  $\omega(A_g) = 513 \text{ cm}^{-1}$ , and the double  $A_g$ , and  $B_{2g}$  peaks at  $\omega(A_g) = 658 \text{ cm}^{-1}$  and  $\omega(B_{2g}) = 668 \text{ cm}^{-1}$ , respectively. Finally, in brookite the  $A_g$  mode ( $\omega(A_g) = 384 \text{ cm}^{-1}$ ) can be used as its fingerprint.

Additionally, we find a signature mode for antipolar polymorphs. This is the high frequency  $B_{1g}$  peak ( $\omega(B_{1g}) = 811 \text{ cm}^{-1}$  for brookite, or  $\omega(B_{1g}) = 791 \text{ cm}^{-1}$  for  $\text{Pbca}$  OI). This mode is absent in the FE ( $\text{Pca}2_1$  and  $\text{Pmn}2_1$ ) structures and it is an anti-phase vibration of the O atoms in neighboring cells of the  $\text{Pbca}$  (Fig.3). This anti-phase vibration of the O atoms can be thought as an anti-phase collective motion of the dipole moments.

The splitting between longitudinal optical (LO) and transverse optical (TO) phonon modes is a subject of interest in ferroelectrics. Indeed, perovskite ferroelectrics are known to have phonon modes that exhibit giant LO-TO splittings<sup>32</sup>. Using the rigorous definition of LO-TO splitting<sup>33</sup>, we show that these large LO-TO splittings also occur in hafnia. In polar  $\text{Pmn}2_1$  phase, the calcu-



used to compute the frequency difference (Fig.4). The modes chosen (Fig. 1, and Fig.2) were modes with non-negligible Raman or IR intensities and the ones showing monotonic behavior if possible, within a range of 200  $\text{cm}^{-1}$  for plotting purposes. In Fig.4 we used results from studies with samples that are either under hydrostatic pressure<sup>31</sup> or doped hafnia<sup>35</sup> for comparison. For the case where doping helps with the stabilization of a particular polymorph, peaks associated to defects or dopants were identified<sup>35</sup> so the comparison with the remaining peaks, probably from the tetragonal polymorph, with our calculation results can be made.

For the comparison of Pbca brookite spectra, the Raman spectra in Ref.31 were obtained under hydrostatic pressure. We performed two different first-principles calculations for the brookite phase, one at ambient pressure and one under 5.9 GPa. We find that pressure hardens the individual Raman modes, as expected. But the difference between two modes ( $\Delta\omega_{l,n}$ ) for the system at ambient pressure was similar to  $\Delta\omega_{l,n}$  for the system under hydrostatic pressure. It is thus fair to compare  $\Delta\omega_{l,n}$  from the experiment under pressure with  $\Delta\omega_{l,n}$  from DFPT at ambient pressure (Fig.4f).

For most cases, the frequency difference between two peaks changes linearly with strain, such as  $\Delta\omega_{B_{1g},B_{2g}}(\eta) = 80 + 4.2\eta$  for the Raman active modes chosen in brookite or  $\Delta\omega_{A_2,B_2}(\eta) = 89 + 5.9\eta$  for the Raman active modes chosen in Pmn2<sub>1</sub>. On the other hand, for the Pca2<sub>1</sub> and baddeleyite the frequency difference is better described by a quadratic polynomial of the strain  $\eta$ :

$$\Delta\omega_{A_g,B_g}(\eta) = 142 - 13.7\eta + 2\eta^2, \quad (4)$$

for the Raman active modes chosen in baddeleyite, and

$$\Delta\omega_{A_1,B_1}(\eta) = 15 + 14.1\eta + 3.7\eta^2 \quad (5)$$

for Pca2<sub>1</sub>.

Now we briefly discuss an interesting comparison between hafnia and zirconia, two isomorphous compounds<sup>3</sup>. Recent studies on ZrO<sub>2</sub> combined experimental measurements and computations of Raman spectra to identify the zirconia polymorphs using Raman<sup>36</sup>. The Raman spectra of monoclinic hafnia and zirconia are similar, e.g. the  $A_g$  peak at  $\omega(A_g) = 495 \text{ cm}^{-1}$  in hafnia and the  $A_g$  peak at  $\omega(A_g) = 470 \text{ cm}^{-1}$  in zirconia, or the  $B_g$  peak at  $\omega(B_g) = 637 \text{ cm}^{-1}$  in hafnia compared to  $\omega(B_g) = 598 \text{ cm}^{-1}$  in zirconia. The quantitative mismatch between the spectra in hafnia and zirconia (25  $\text{cm}^{-1}$  for  $A_g$  and 30  $\text{cm}^{-1}$  for  $B_g$ ) can be attributed to differences in the interatomic force constant (IFC) resulting from the difference in the cation. Interestingly, despite these quantitative discrepancies in the Raman frequencies of hafnia and zirconia, the frequency differences  $\Delta\omega_{l,n}$  are comparable. In monoclinic hafnia for example, the frequency difference  $\Delta\omega_{A_g,B_g} = 142 \text{ cm}^{-1}$  compares well with  $\Delta\omega_{A_g,B_g} = 140 \text{ cm}^{-1}$  in zirconia, and in tetragonal the frequency difference  $\Delta\omega_{E_g,B_{1g}} = 130 \text{ cm}^{-1}$  in hafnia is a close match to  $\Delta\omega_{E_g,B_{1g}} = 135 \text{ cm}^{-1}$  in zirconia.

We computed the phonon frequencies of P4<sub>2</sub>nmc, Pmn2<sub>1</sub>, Pca2<sub>1</sub>, Pbca (OI), brookite, and baddeleyite using DFPT at different values of epitaxial strains. We found that Raman spectra can be used to identify the symmetry or phases of hafnia, namely  $\omega(A_{1g}) = 300 \text{ cm}^{-1}$  for P4<sub>2</sub>nmc,  $\omega(A_1) = 343 \text{ cm}^{-1}$  for Pca2<sub>1</sub>,  $\omega(B_2) = 693 \text{ cm}^{-1}$  for Pmn2<sub>1</sub>,  $\omega(A_g) = 513 \text{ cm}^{-1}$  for Pbca (OI),  $\omega(A_g) = 384 \text{ cm}^{-1}$  for brookite, and  $\omega(A_g) = 496 \text{ cm}^{-1}$  for baddeleyite. We also identified the Raman signature of AFE structures as the  $\omega(B_{1g}) = 784 \text{ cm}^{-1}$  peak for brookite or the  $\omega(B_{1g}) = 758 \text{ cm}^{-1}$  peak for Pbca (OI). The presence (or absence) of this Raman signal can be used to distinguish between AFE and FE orthorhombic hafnia. Further, we showed the evolution of frequency differences between selected normal mode frequencies with respect to strain for calibration purposes and identification of strain state of the hafnia crystal.

## SUPPLEMENTARY MATERIAL

Comparison of brookite Raman spectra at ambient pressure (Fig.S1), the calculated Born effective charges (Table S1–S2), the infrared frequencies and IR activities of different hafnia polymorphs (Table S3–S8).

## ACKNOWLEDGMENTS

The authors thank Pavlo Zubko for helpful discussions. This work is supported by U. S. Office of Naval Research Grants No. N00014-17-1-2768 and N00014-20-1-2699, and the Carnegie Institution for Science. Computations were supported by DOD HPC, Carnegie computational resources, and REC gratefully acknowledges the Gauss Centre for Supercomputing e.V. ([www.gauss-center.eu](http://www.gauss-center.eu)) for funding this project by providing computing time on the GCS Supercomputer SuperMUC-NG at Leibniz Supercomputing Centre (LRZ, [www.lrz.de](http://www.lrz.de)). Some of the computing for this project was performed on the Memex cluster. We would like to thank Carnegie Institution for Science and the Carnegie Sci-Comp Committee for providing computational resources and support that contributed to these research results.

<sup>1</sup>A. I. Kingon, J.-P. Maria, and S. K. Streiffer, “Alternative dielectrics to silicon dioxide for memory and logic devices,” *Nature* **406**, 1032–1038 (2000).

<sup>2</sup>G. D. Wilk, R. M. Wallace, and J. M. Anthony, “High-gate dielectrics: Current status and materials properties considerations,” *Journal of Applied Physics* **89**, 5243–5275 (2001).

<sup>3</sup>R. Ruh and P. W. R. Corfield, “Crystal Structure of Monoclinic Hafnia and Comparison with Monoclinic Zirconia,” *Journal of the American Ceramic Society* **53**, 126–129 (1970).

<sup>4</sup>O. Ohtaka, H. Fukui, T. Kunisada, T. Fujisawa, K. Funakoshi, W. Utsumi, T. Irifune, K. Kuroda, and T. Kikegawa, “Phase relations and volume changes of hafnia under high pressure and high temperature,” *Journal of the American Ceramic Society* **84**, 1369–1373 (2001).

- <sup>5</sup>T. D. Huan, V. Sharma, G. A. Rossetti, and R. Ramprasad, “Pathways Towards Ferroelectricity in Hafnia,” *Phys. Rev. B* **90**, 064111 (2014).
- <sup>6</sup>S. Liu and B. M. Hanrahan, “Effects of Growth Orientations and Epitaxial Strains on Phase Stability of HfO<sub>2</sub> Thin Films,” *Physical Review Materials* **3**, 054404 (2019).
- <sup>7</sup>M. H. Park, T. Schenk, C. M. Fancher, E. D. Grimley, C. Zhou, C. Richter, J. M. LeBeau, J. L. Jones, T. Mikolajick, and U. Schroeder, “A comprehensive study on the structural evolution of HfO<sub>2</sub> thin films doped with various dopants,” *J. Mater. Chem. C* **5**, 4677–4690 (2017).
- <sup>8</sup>R. Batra, T. D. Huan, G. A. Rossetti, and R. Ramprasad, “Dopants Promoting Ferroelectricity in Hafnia: Insights from a comprehensive Chemical Space Exploration,” *Chemistry of Materials* **29**, 9102–9109 (2017).
- <sup>9</sup>T. S. Böscke, J. Müller, D. Bräuhaus, U. Schröder, and U. Böttger, “Ferroelectricity in Hafnium Oxide Thin Films,” *Applied Physics Letters* **99**, 102903 (2011).
- <sup>10</sup>U. Schroeder, C. Hwang, and H. Funakubo, *Ferroelectricity in Doped Hafnium Oxide: Materials, Properties and Devices*, Woodhead Publishing Series in Electronic and Optical Materials (Elsevier Science, 2019).
- <sup>11</sup>H.-J. Lee, M. Lee, K. Lee, J. Jo, H. Yang, Y. Kim, S. C. Chae, U. Waghmare, and J. H. Lee, “Scale-free Ferroelectricity Induced by Flat Phonon Bands in HfO<sub>2</sub>,” *Science* **369**, 1343–1347 (2020).
- <sup>12</sup>Y. Qi, S. Singh, C. Lau, F.-T. Huang, X. Xu, F. J. Walker, C. H. Ahn, S.-W. Cheong, and K. M. Rabe, “Stabilization of Competing Ferroelectric Phases of HfO<sub>2</sub> Under Epitaxial Strain,” *Phys. Rev. Lett.* **125**, 257603 (2020).
- <sup>13</sup>X. Xu, F.-T. Huang, Y. Qi, S. Singh, K. M. Rabe, D. Obeysekera, J. Yang, M.-W. Chu, and S.-W. Cheong, “Kinetically Stabilized Ferroelectricity in Bulk Single-Crystalline HfO<sub>2</sub>:Y,” *Nature Materials* **20**, 826–832 (2021).
- <sup>14</sup>T. Mikolajick and U. Schroeder, “Ferroelectricity in Bulk Hafnia,” *Nature Materials* **20**, 718–719 (2021).
- <sup>15</sup>J. Müller, U. Schröder, T. S. Böscke, I. Müller, U. Böttger, L. Wilde, J. Sundqvist, M. Lemberger, P. Kücher, T. Mikolajick, and L. Frey, “Ferroelectricity in yttrium-doped hafnium oxide,” *Journal of Applied Physics* **110**, 114113 (2011).
- <sup>16</sup>M. H. Park, Y. H. Lee, H. J. Kim, Y. J. Kim, T. Moon, K. D. Kim, J. Miller, A. Kersch, U. Schroeder, T. Mikolajick, and C. S. Hwang, “Ferroelectricity and antiferroelectricity of doped thin hfo<sub>2</sub>-based films,” *Advanced Materials* **27**, 1811–1831 (2015).
- <sup>17</sup>B. Zhou, H. Shi, X. D. Zhang, Q. Su, and Z. Y. Jiang, “The Simulated Vibrational Spectra of HfO<sub>2</sub> Polymorphs,” *Journal of Physics D: Applied Physics* **47**, 115502 (2014).
- <sup>18</sup>T. Gunst, D. Stradi, and A. Blom, “Identification of zirconia and hafnia crystalline phases by optical spectroscopy from first-principles,” in *Nanoengineering: Fabrication, Properties, Optics, Thin Films, and Devices XVII*, Vol. 11467, edited by B. Panchapakesan, A.-J. Attias, and W. Park, International Society for Optics and Photonics (SPIE, 2020) pp. 34–47.
- <sup>19</sup>S. Fan, S. Singh, X. Xu, K. Park, Y. Qi, a. V. S.W. Cheong, K. M. Rabe, and J. L. Musfeldt, “Vibrational fingerprints of ferroelectric hafnia,” arXiv:2201.12643.
- <sup>20</sup>V. Mukundan, S. Consiglio, D. H. Triyoso, K. Tapily, M. E. McBriarty, S. Schujman, K. Beckmann, J. Hazra, V. Kaushik, N. Cady, R. D. Clark, G. J. Leusink, and A. C. Diebold, “Ferroelectric Phase Content in 7nm Hf<sub>(1-x)</sub>Zr<sub>x</sub>O<sub>2</sub> Thin Films Determined by X-Ray-Based Methods,” *physica status solidi (a)* **218**, 2100024 (2021).
- <sup>21</sup>P. Giannozzi, S. Baroni, N. Bonini, M. Calandra, R. Car, C. Cavazzoni, D. Ceresoli, G. L. Chiarotti, M. Cococcioni, I. Dabo, A. Dal Corso, S. de Gironcoli, S. Fabris, G. Fratesi, R. Gebauer, U. Gerstmann, C. Gougoussis, A. Kokalj, M. Lazzeri, L. Martin-Samos, N. Marzari, F. Mauri, R. Mazzeo, S. Paolini, A. Pasquarello, L. Paulatto, C. Sbraccia, S. Scandolo, G. Sclauzero, A. P. Seitsonen, A. Smogunov, P. Umari, and R. M. Wentzcovitch, “QUANTUM ESPRESSO: A Modular and Open-Source Software Project for Quantum Simulations of Materials,” *Journal of Physics: Condensed Matter* **21**, 395502 (2009).
- <sup>22</sup>P. Giannozzi, O. Andreussi, T. Brumme, O. Bunau, M. B. Nardelli, M. Calandra, R. Car, C. Cavazzoni, D. Ceresoli, M. Cococcioni, N. Colonna, I. Carnimeo, A. D. Corso, S. de Gironcoli, P. Delugas, R. A. D. Jr, A. Ferretti, A. Floris, G. Fratesi, G. Fugallo, R. Gebauer, U. Gerstmann, F. Giustino, T. Gorni, J. Jia, M. Kawamura, H.-Y. Ko, A. Kokalj, E. Kkbenli, M. Lazzeri, M. Marsili, N. Marzari, F. Mauri, N. L. Nguyen, H.-V. Nguyen, A. O. de-la Roza, L. Paulatto, S. Ponc, D. Rocca, R. Sabatini, B. Santra, M. Schlipf, A. P. Seitsonen, A. Smogunov, I. Timrov, T. Thonhauser, P. Umari, N. Vast, X. Wu, and S. Baroni, “Advanced Capabilities for Materials Modelling With QUANTUM ESPRESSO,” *Journal of Physics: Condensed Matter* **29**, 465901 (2017).
- <sup>23</sup>P. Giannozzi, O. Baseggio, P. Bonf, D. Brunato, R. Car, I. Carnimeo, C. Cavazzoni, S. de Gironcoli, P. Delugas, F. Ferrari Ruffino, A. Ferretti, N. Marzari, I. Timrov, A. Urru, and S. Baroni, “Quantum ESPRESSO Toward the Exascale,” *The Journal of Chemical Physics* **152**, 154105 (2020).
- <sup>24</sup>D. R. Hamann, “Optimized Norm-Conserving Vanderbilt Pseudopotentials,” *Phys. Rev. B* **88**, 085117 (2013).
- <sup>25</sup>J. P. Perdew and A. Zunger, “Self-Interaction Correction to Density-Functional Approximations for Many-Electron Systems,” *Phys. Rev. B* **23**, 5048–5079 (1981).
- <sup>26</sup>H. J. Monkhorst and J. D. Pack, “Special Points for Brillouin-Zone Integrations,” *Phys. Rev. B* **13**, 5188–5192 (1976).
- <sup>27</sup>S. Baroni, S. de Gironcoli, A. Dal Corso, and P. Giannozzi, “Phonons and Related Crystal Properties from Density-Functional Perturbation Theory,” *Rev. Mod. Phys.* **73**, 515–562 (2001).
- <sup>28</sup>D. Porezag and M. R. Pederson, “Infrared intensities and raman-scattering activities within density-functional theory,” *Phys. Rev. B* **54**, 7830–7836 (1996).
- <sup>29</sup>M. Lazzeri and F. Mauri, “First-Principles Calculation of Vibrational Raman Spectra in Large Systems: Signature of Small Rings in Crystalline sio<sub>2</sub>,” *Phys. Rev. Lett.* **90**, 036401 (2003).
- <sup>30</sup>R. Caracas and R. E. Cohen, “Theoretical determination of the Raman spectra of MgSiO<sub>3</sub>perovskite and post-perovskite at high pressure,” *Geophysical Research Letters* **33** (2006), <https://doi.org/10.1029/2006GL025736>.
- <sup>31</sup>A. Jayaraman, S. Y. Wang, S. K. Sharma, and L. C. Ming, “Pressure-induced Phase Transformations in HfO<sub>2</sub> to 50 GPa studied by Raman spectroscopy,” *Physical Review B* **48**, 9205–9211 (1993).
- <sup>32</sup>W. Zhong, R. D. King-Smith, and D. Vanderbilt, “Giant lo-to splittings in perovskite ferroelectrics,” *Phys. Rev. Lett.* **72**, 3618–3621 (1994).
- <sup>33</sup>A. Raeliarijaona and H. Fu, “ModeSequence, Frequency Change of Nonsoft Phonons, and LO-TO Splitting in strained tetragonal batio<sub>3</sub>,” *Phys. Rev. B* **92**, 094303 (2015).
- <sup>34</sup>S. N. Neal, S. Li, T. Birol, and J. L. Musfeldt, “Chemical bonding and Born charge in 1T-HfS<sub>2</sub>,” *npj 2D Materials and Applications* **5**, 45 (2021).
- <sup>35</sup>Y. Masatomo, T. H., O. Katsuya, H. Teruo, K. Masato, A. Haruo, I. Yasuro, S. Yasuo, and Y. Masahiro, “Formation of Metastable Forms by Quenching of the HfO<sub>2</sub>RO<sub>1.5</sub> Melts (R = Gd, Y and Yb),” *Journal of Physics and Chemistry of Solids* **57**, 289–295 (1996).
- <sup>36</sup>M. Materano, P. Reinig, A. Kersch, M. Popov, M. Deluca, T. Mikolajick, U. Boettger, and U. Schroeder, “Raman Spectroscopy as a Key Method to Distinguish the Ferroelectric Orthorhombic Phase in Thin ZrO<sub>2</sub>-Based Films,” *Physica Status Solidi (RRL) Rapid Research Letters* **16**, 2100589 (2022).

# Supplementary Material: First-principles Calculations of Raman and Infrared Spectroscopy For Phase Identification and Strain Calibration of Hafnia.

## A. Comparison of Raman spectra

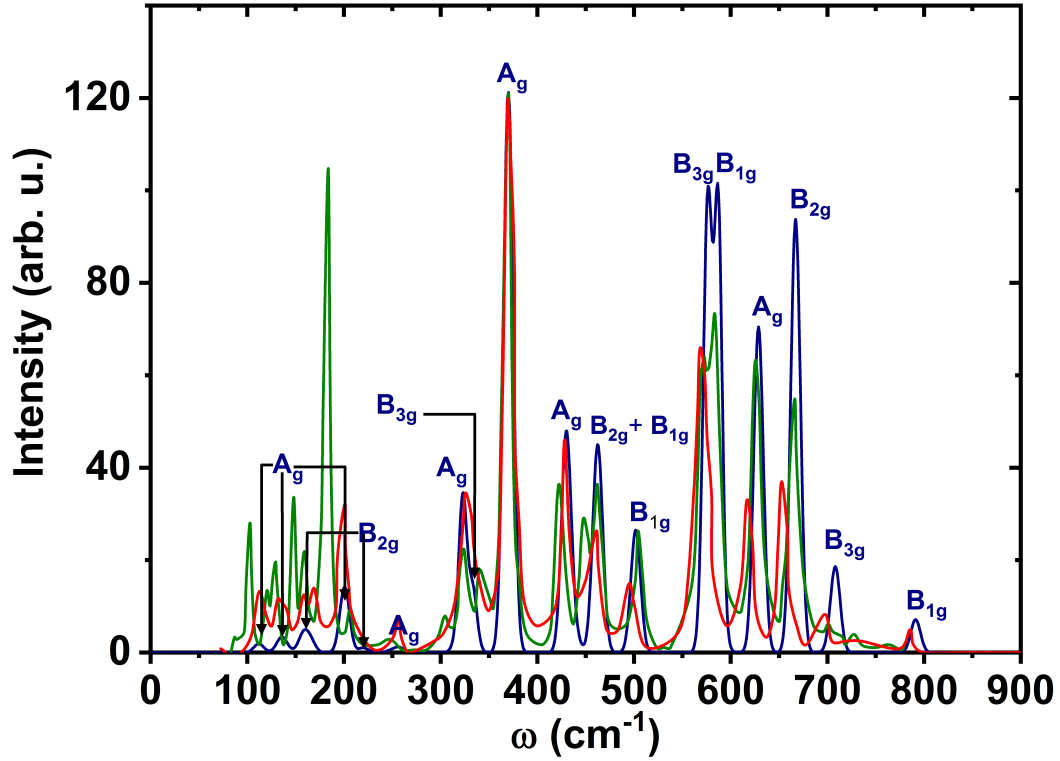


FIG. S1. Calculated Raman spectrum of brookite (blue) compared to theoretical Raman spectrum (red)<sup>S1</sup> at ambient pressure. The calculated spectrum was convoluted with a Gaussian shape function of width  $5 \text{ cm}^{-1}$  estimated from experiments.

## B. Born effective charges

Phase	Atoms	$Z_{xx}^*$	$Z_{xy}^*$	$Z_{xz}^*$	$Z_{yx}^*$	$Z_{yy}^*$	$Z_{yz}^*$	$Z_{zx}^*$	$Z_{zy}^*$	$Z_{zz}^*$	Nominal charge
Baddeleyite	Hf1	5.33	-0.39	0.23	-0.12	5.34	0.15	0.24	0.35	4.75	4
	Hf2	5.33	0.39	0.23	0.12	5.34	-0.15	0.24	-0.35	4.75	4
	O1	-2.95	-1.05	-0.22	-1.30	-2.60	0.64	-0.19	0.63	-2.22	-2
	O2	-2.95	1.05	-0.22	1.30	-2.60	-0.64	-0.19	-0.63	-2.22	-2
	O3	-2.37	-0.11	-0.01	-0.18	-2.74	-0.35	-0.05	-0.42	-2.53	-2
	O4	-2.37	0.11	-0.01	0.18	-2.74	0.35	-0.05	0.42	-2.53	-2
P4 <sub>2</sub> nmc	Hf	5.54	0	0	0	5.54	0	0	0	4.84	4
	O1	-2.12	0	0	0	-3.42	0	0	0	-2.42	-2
	O2	-3.42	0	0	0	-2.12	0	0	0	-2.42	-2
Pmn2 <sub>1</sub>	Hf1	5.35	0	0	0	5.02	0.10	0	0.33	5.11	4
	Hf2	5.35	0	0	0	5.02	-0.10	0	-0.33	5.11	4
	O1	-3.15	0	0	0	-2.67	-0.80	0	-0.86	-2.03	-2
	O2	-3.15	0	0	0	-2.67	0.80	0	0.86	-2.03	-2
	O3	-2.20	0	0	0	-2.35	0.04	0	-0.05	-3.08	-2
	O4	-2.20	0	0	0	-2.35	-0.04	0	0.05	-3.08	-2

TABLE S1. Computed Born effective charges for baddeleyite, P4<sub>2</sub>nmc and Pmn2<sub>1</sub> hafnia polymorphs compared to their nominal charges. Hf1, Hf2 (resp. O1, O2, O3, and O4) are the symmetrically inequivalent Hf (resp. O) atoms in the HfO<sub>2</sub> unit cell.

## C. IR frequencies

Here we list the computed IR frequencies, their intensities and their symmetry.

Phase	Atoms	$Z_{xx}^*$	$Z_{xy}^*$	$Z_{xz}^*$	$Z_{yx}^*$	$Z_{yy}^*$	$Z_{yz}^*$	$Z_{zx}^*$	$Z_{zy}^*$	$Z_{zz}^*$	Nominal charge
Pca2 <sub>1</sub>	Hf1	5.17	0.00	-0.035	-0.35	5.49	-0.14	0.05	-0.22	4.97	4
	Hf2	5.17	0.00	0.035	-0.35	5.49	0.14	-0.05	0.22	4.97	4
	Hf3	5.17	0.00	-0.035	0.35	5.49	0.14	0.05	0.22	4.97	4
	Hf4	5.17	0.00	0.035	0.35	5.49	-0.14	-0.05	-0.22	4.97	4
	O1	-2.49	-0.96	0.31	-0.76	-2.96	-0.69	0.31	-0.63	-2.46	-2
	O2	-2.49	-0.96	-0.31	-0.76	-2.96	0.69	-0.31	0.63	-2.46	-2
	O3	-2.49	0.96	0.31	0.76	-2.96	0.69	0.31	0.63	-2.46	-2
	O4	-2.49	0.96	-0.31	0.76	-2.96	-0.69	-0.31	-0.63	-2.46	-2
	O5	-2.68	0.13	0.25	0.07	-2.52	-0.19	0.29	-0.13	-2.50	-2
	O6	-2.68	0.13	-0.25	0.07	-2.52	0.19	-0.29	0.13	-2.50	-2
	O7	-2.68	-0.13	0.25	-0.07	-2.52	0.19	0.29	0.13	-2.50	-2
	O8	-2.68	-0.13	-0.25	-0.07	-2.52	-0.19	-0.29	-0.13	-2.50	-2
Pbca (OI)	Hf1	5.28	0.34	0.13	0.34	4.78	-0.03	0.30	-0.08	5.43	4
	Hf2	5.28	0.34	-0.13	0.34	4.78	0.03	-0.30	0.08	5.43	4
	Hf3	5.28	-0.34	0.13	-0.34	4.78	0.03	0.30	0.08	5.43	4
	Hf4	5.28	-0.34	-0.13	-0.34	4.78	-0.03	-0.30	-0.08	5.43	4
	O1	-2.56	-0.87	-1.14	-0.87	-2.23	0.01	-0.89	0.10	-3.02	-2
	O2	-2.56	-0.87	1.14	-0.87	-2.23	-0.01	0.89	-0.10	-3.02	-2
	O3	-2.56	0.87	-1.14	0.87	-2.23	-0.01	-0.89	-0.10	-3.02	-2
	O4	-2.56	0.87	1.14	0.87	-2.23	0.01	0.89	0.10	-3.02	-2
	O5	-2.73	0.28	-0.12	0.41	-2.55	-0.10	-0.07	-0.02	-2.41	-2
	O6	-2.73	0.28	0.12	0.41	-2.55	0.10	0.07	0.02	-2.41	-2
	O7	-2.73	-0.28	-0.12	-0.41	-2.55	0.10	-0.07	0.02	-2.41	-2
	O8	-2.73	-0.28	0.12	-0.41	-2.55	-0.10	0.07	-0.02	-2.41	-2
Brookite	Hf1	4.89	0.24	-0.02	0.04	5.46	0.39	-0.13	-0.00	5.31	4
	Hf2	4.89	0.24	0.02	0.04	5.46	-0.39	0.13	0.00	5.31	4
	Hf3	4.89	-0.24	-0.02	-0.04	5.46	-0.39	-0.13	0.00	5.31	4
	Hf4	4.89	-0.24	0.02	-0.04	5.46	0.39	0.13	-0.00	5.31	4
	O1	-2.49	-0.04	0.36	-0.09	-2.49	0.04	0.31	0.01	-2.76	-2
	O2	-2.49	-0.04	-0.36	-0.09	-2.49	-0.04	-0.31	-0.01	-2.76	-2
	O3	-2.49	0.04	0.36	0.09	-2.49	-0.04	0.31	-0.01	-2.76	-2
	O4	-2.49	0.04	-0.36	0.09	-2.49	0.04	-0.31	0.01	-2.76	-2
	O5	-2.39	-0.56	0.31	-0.62	-2.97	-0.80	0.32	-0.98	-2.55	-2
	O6	-2.39	-0.56	-0.31	-0.62	-2.97	0.80	-0.32	0.98	-2.55	-2
	O7	-2.39	0.56	0.31	0.62	-2.97	0.80	0.32	0.98	-2.55	-2
	O8	-2.39	0.56	-0.31	0.62	-2.97	-0.80	-0.32	-0.98	-2.55	-2

TABLE S2. Computed Born effective charges for Pca2<sub>1</sub>, Pbca (OI) and brookite hafnia polymorphs compared to their nominal charges. Hf1, Hf2, Hf3 and Hf4 (resp. O1, O2, O3, and O4) are the symmetrically inequivalent Hf (resp. O) atoms in the HfO<sub>2</sub> unit cell.

	Mode	Freq (cm <sup>-1</sup> )	IR (arb. u.)		Mode	Freq (cm <sup>-1</sup> )	IR (arb. u.)		Mode	Freq (cm <sup>-1</sup> )	IR (arb. u.)
q → [001]	B <sub>u</sub>	236	22.84	q → [010]	B <sub>u</sub>	232	20.07	q → [100]	B <sub>u</sub>	249	5.72
	A <sub>u</sub>	256	20.18		B <sub>u</sub>	311	64.83		A <sub>u</sub>	256	20.18
	B <sub>u</sub>	320	41.87		B <sub>u</sub>	345	24.74		B <sub>u</sub>	256	2.02
	A <sub>u</sub>	361	39.70		B <sub>u</sub>	405	40.35		B <sub>u</sub>	345	23.81
	B <sub>u</sub>	370	7.43		A <sub>u</sub>	476	2.40		A <sub>u</sub>	361	39.70
	A <sub>u</sub>	411	24.29		B <sub>u</sub>	520	19.66		B <sub>u</sub>	400	49.06
	A <sub>u</sub>	499	12.55		A <sub>u</sub>	575	9.21		A <sub>u</sub>	411	24.29
	B <sub>u</sub>	516	19.40		B <sub>u</sub>	741	14.87		B <sub>u</sub>	455	9.53
	A <sub>u</sub>	614	12.53		A <sub>u</sub>	750	96.89		A <sub>u</sub>	499	12.55
	B <sub>u</sub>	651	76.23						A <sub>u</sub>	614	12.53
B <sub>u</sub>	743	16.88				B <sub>u</sub>	623	34.20			
						B <sub>u</sub>	813	60.68			

TABLE S3. Frequencies of IR-active modes in baddeleyite. Modes colored in blue are the modes used to compute frequency differences (see text).

	Mode	Freq (cm <sup>-1</sup> )	IR (arb. u.)		Mode	Freq (cm <sup>-1</sup> )	IR (arb. u.)		Mode	Freq (cm <sup>-1</sup> )	IR (arb. u.)
q → [001]	E <sub>u</sub>	95	19.57	q → [010]	E <sub>u</sub>	95	19.57	q → [100]	E <sub>u</sub>	95	19.57
	E <sub>u</sub>	95	19.57		E <sub>u</sub>	246	2.62		E <sub>u</sub>	246	2.62
	E <sub>u</sub>	462	35.04		A <sub>2u</sub>	324	39.86		A <sub>2u</sub>	324	39.86
	E <sub>u</sub>	462	35.04		E <sub>u</sub>	462	35.04		E <sub>u</sub>	462	35.04
	A <sub>2u</sub>	627	39.86		E <sub>u</sub>	720	51.99		E <sub>u</sub>	720	51.99

TABLE S4. Frequencies of IR-active modes for P4<sub>2</sub>nmc . Modes colored in blue are the modes used to compute frequency differences (see text).

	Mode	Freq (cm <sup>-1</sup> )	IR (arb. u.)		Mode	Freq (cm <sup>-1</sup> )	IR (arb. u.)		Mode	Freq (cm <sup>-1</sup> )	IR (arb. u.)
q → [001]	B <sub>2</sub>	250	25.10	q → [010]	A <sub>1</sub>	177	6.80	q → [100]	A <sub>1</sub>	177	6.80
	B <sub>1</sub>	300	32.60		B <sub>2</sub>	250	25.10		A <sub>1</sub>	254	3.80
	B <sub>2</sub>	451	24.87		A <sub>1</sub>	254	3.80		B <sub>1</sub>	300	32.60
	B <sub>1</sub>	492	10.10		A <sub>1</sub>	364	2.93		B <sub>2</sub>	345	2.01
	A <sub>1</sub>	587	3.01		B <sub>1</sub>	432	3.06		A <sub>1</sub>	364	2.93
	B <sub>1</sub>	701	2.10		A <sub>1</sub>	451	31.75		A <sub>1</sub>	451	31.75
	A <sub>1</sub>	722	43.82		B <sub>2</sub>	451	24.87		B <sub>1</sub>	492	10.10
					A <sub>1</sub>	606	2.84		A <sub>1</sub>	606	2.84
			B <sub>1</sub>	632	20.16	B <sub>2</sub>	692	47.97			
			B <sub>1</sub>	738	20.90	B <sub>1</sub>	701	2.10			

TABLE S5. Frequencies of IR-active modes for Pmn2<sub>1</sub> . Modes colored in blue are the modes used to compute frequency differences (see text).

	Mode	Freq (cm <sup>-1</sup> )	IR (arb. u.)		Mode	Freq (cm <sup>-1</sup> )	IR (arb. u.)		Mode	Freq (cm <sup>-1</sup> )	IR (arb. u.)
q → [001]	B <sub>1</sub>	144	1.06	q → [010]	A <sub>1</sub>	122	2.18	q → [100]	A <sub>1</sub>	122	2.18
	B <sub>1</sub>	237	40.77		A <sub>1</sub>	163	8.47		B <sub>1</sub>	144	1.06
	B <sub>1</sub>	248	1.29		A <sub>1</sub>	260	2.19		A <sub>1</sub>	163	8.47
	B <sub>2</sub>	275	37.59		B <sub>2</sub>	275	37.59		B <sub>1</sub>	237	40.77
	B <sub>2</sub>	335	2.14		B <sub>1</sub>	305	2.09		B <sub>1</sub>	248	1.29
	B <sub>2</sub>	393	50.69		A <sub>1</sub>	333	5.98		A <sub>1</sub>	260	2.19
	B <sub>1</sub>	397	49.25		B <sub>2</sub>	335	2.14		A <sub>1</sub>	333	5.98
	A <sub>1</sub>	431	3.16		A <sub>1</sub>	342	46.83		A <sub>1</sub>	342	46.83
	B <sub>2</sub>	490	1.94		B <sub>2</sub>	393	50.69		B <sub>1</sub>	397	49.25
	B <sub>1</sub>	532	8.19		A <sub>1</sub>	471	19.92		A <sub>1</sub>	471	19.92
	A <sub>1</sub>	593	8.10		B <sub>2</sub>	490	1.94		B <sub>1</sub>	532	8.19
	B <sub>2</sub>	644	3.79		B <sub>1</sub>	510	4.39		A <sub>1</sub>	606	1.95
	A <sub>1</sub>	676	75.48		A <sub>1</sub>	606	1.95		B <sub>2</sub>	610	22.60
B <sub>1</sub>	747	7.78	B <sub>2</sub>	644	3.79	B <sub>2</sub>	692	22.93			
				B <sub>1</sub>	652	49.35	B <sub>2</sub>	722	50.20		
				B <sub>1</sub>	796	53.18	B <sub>1</sub>	747	7.78		

TABLE S6. Frequencies of IR-active modes for Pca2<sub>1</sub>. Modes colored in blue are the modes used to compute frequency differences (see text).

	Mode	Freq (cm <sup>-1</sup> )	IR (arb. u.)		Mode	Freq (cm <sup>-1</sup> )	IR (arb. u.)		Mode	Freq (cm <sup>-1</sup> )	IR (arb. u.)
q → [001]	B <sub>3u</sub>	249	15.35	q → [010]	B <sub>1u</sub>	233	15.82	q → [100]	B <sub>1u</sub>	233	15.82
	B <sub>2u</sub>	266	43.84		B <sub>1u</sub>	262	9.72		B <sub>3u</sub>	249	15.35
	B <sub>3u</sub>	313	9.06		B <sub>2u</sub>	266	43.84		B <sub>1u</sub>	262	9.72
	B <sub>2u</sub>	323	56.19		B <sub>1u</sub>	296	115.67		B <sub>1u</sub>	296	115.67
	B <sub>3u</sub>	379	127.96		B <sub>2u</sub>	323	56.19		B <sub>3u</sub>	313	9.06
	B <sub>2u</sub>	386	64.30		B <sub>1u</sub>	358	20.51		B <sub>2u</sub>	353	1.43
	B <sub>3u</sub>	454	4.70		B <sub>2u</sub>	386	64.30		B <sub>1u</sub>	358	20.51
	B <sub>1u</sub>	471	16.78		B <sub>2u</sub>	512	30.16		B <sub>3u</sub>	379	127.96
	B <sub>3u</sub>	477	7.51		B <sub>1u</sub>	515	22.85		B <sub>3u</sub>	454	4.70
	B <sub>2u</sub>	512	30.16		B <sub>1u</sub>	580	2.29		B <sub>2u</sub>	476	8.89
	B <sub>1u</sub>	573	7.54		B <sub>2u</sub>	617	19.59		B <sub>3u</sub>	477	7.51
	B <sub>2u</sub>	617	19.59		B <sub>3u</sub>	653	154.48		B <sub>1u</sub>	515	22.85
	B <sub>1u</sub>	623	73.73		B <sub>1u</sub>	742	25.26		B <sub>1u</sub>	580	2.29
	B <sub>1u</sub>	805	113.23		B <sub>3u</sub>	811	9.98		B <sub>2u</sub>	584	17.46
	B <sub>3u</sub>	806	2.00						B <sub>2u</sub>	669	2.11
									B <sub>1u</sub>	742	25.26
									B <sub>2u</sub>	742	184.42
						B <sub>3u</sub>	806	2.00			

TABLE S7. Frequencies of IR-active modes in Pbca OI. Modes colored in blue are the modes used to compute frequency differences (see text).

	Mode	Freq (cm <sup>-1</sup> )	IR (arb. u.)		Mode	Freq (cm <sup>-1</sup> )	IR (arb. u.)		Mode	Freq (cm <sup>-1</sup> )	IR (arb. u.)
q → [001]	B <sub>2u</sub>	191	17.37	q → [010]	B <sub>2u</sub>	191	17.37	q → [100]	B <sub>3u</sub>	253	8.16
	B <sub>2u</sub>	224	5.85		B <sub>2u</sub>	224	5.85		B <sub>3u</sub>	263	79.64
	B <sub>3u</sub>	253	8.16		B <sub>1u</sub>	280	71.48		B <sub>1u</sub>	280	71.48
	B <sub>3u</sub>	263	79.64		B <sub>3u</sub>	319	2.92		B <sub>3u</sub>	385	88.62
	B <sub>1u</sub>	323	2.28		B <sub>2u</sub>	363	51.56		B <sub>1u</sub>	392	82.96
	B <sub>2u</sub>	363	51.56		B <sub>2u</sub>	368	55.47		B <sub>2u</sub>	423	1.81
	B <sub>2u</sub>	368	55.47		B <sub>1u</sub>	392	82.96		B <sub>1u</sub>	425	33.01
	B <sub>3u</sub>	385	88.62		B <sub>1u</sub>	425	33.01		B <sub>1u</sub>	506	8.66
	B <sub>2u</sub>	441	30.44		B <sub>2u</sub>	441	30.44		B <sub>3u</sub>	555	21.39
	B <sub>1u</sub>	499	1.97		B <sub>1u</sub>	506	8.66		B <sub>2u</sub>	571	19.38
	B <sub>3u</sub>	555	21.39		B <sub>3u</sub>	517	16.09		B <sub>1u</sub>	646	7.35
	B <sub>2u</sub>	594	8.16		B <sub>2u</sub>	594	8.16		B <sub>2u</sub>	669	12.62
	B <sub>1u</sub>	620	31.91		B <sub>1u</sub>	646	7.35		B <sub>2u</sub>	683	133.57
	B <sub>1u</sub>	703	66.91		B <sub>3u</sub>	658	85.45		B <sub>1u</sub>	726	2.32
	B <sub>1u</sub>	750	102.39		B <sub>1u</sub>	726	2.32		B <sub>3u</sub>	752	17.74
	B <sub>3u</sub>	752	17.74		B <sub>3u</sub>	808	111.77				

TABLE S8. Frequencies of IR-active modes in brookite. Modes colored in blue are the modes used to compute frequency differences (see text).

## REFERENCES

- [S1]B. Zhou, H. Shi, X. D. Zhang, Q. Su, and Z. Y. Jiang, “The Simulated Vibrational Spectra of HfO<sub>2</sub> Polymorphs,” *Journal of Physics D: Applied Physics* **47**, 115502 (2014).